

Article

Heat-Induced Transformation of Luminescent, Size Tuneable, Anisotropic Eu:Lu(OH)₂Cl Microparticles to Micro-Structurally Controlled Eu:Lu₂O₃ Microplatelets

Madeleine Fellner , Alberto Soppelsa and Alessandro Lauria * 

Laboratory for Multifunctional Materials, Department of Materials, ETH Zürich, Vladimir-Prelog-Weg 5, 8093 Zürich, Switzerland; madeleine.fellner@mat.ethz.ch (M.F.); soppelsa.alberto@gmail.com (A.S.)

* Correspondence: alessandro.lauria@mat.ethz.ch

Abstract: Synthetic procedures to obtain size and shape-controlled microparticles hold great promise to achieve structural control on the microscale of macroscopic ceramic- or composite-materials. Lutetium oxide is a material relevant for scintillation due to its high density and the possibility to dope with rare earth emitter ions. However, rare earth sesquioxides are challenging to synthesise using bottom-up methods. Therefore, calcination represents an interesting approach to transform lutetium-based particles to corresponding sesquioxides. Here, the controlled solvothermal synthesis of size-tuneable europium doped Lu(OH)₂Cl microplatelets and their heat-induced transformation to Eu:Lu₂O₃ above 800 °C are described. The particles obtained in microwave solvothermal conditions, and their thermal evolution were studied using powder X-ray diffraction, scanning electron microscopy (SEM), transmission electron microscopy (TEM), optical microscopy, thermogravimetric analysis (TGA), luminescence spectroscopy (PL/PLE) and infrared spectroscopy (ATR-IR). The successful transformation of Eu:Lu(OH)₂Cl particles into polycrystalline Eu:Lu₂O₃ microparticles is reported, together with the detailed analysis of their initial and final morphology.

Keywords: anisotropy; particle synthesis; luminescence; europium-doping; Lu(OH)₂Cl; Lu₂O₃



Citation: Fellner, M.; Soppelsa, A.; Lauria, A. Heat-Induced Transformation of Luminescent, Size Tuneable, Anisotropic Eu:Lu(OH)₂Cl Microparticles to Micro-Structurally Controlled Eu:Lu₂O₃ Microplatelets. *Crystals* **2021**, *11*, 992. <https://doi.org/10.3390/cryst11080992>

Academic Editor: Alessandra Toncelli

Received: 16 July 2021

Accepted: 17 August 2021

Published: 20 August 2021

Publisher's Note: MDPI stays neutral with regard to jurisdictional claims in published maps and institutional affiliations.



Copyright: © 2021 by the authors. Licensee MDPI, Basel, Switzerland. This article is an open access article distributed under the terms and conditions of the Creative Commons Attribution (CC BY) license (<https://creativecommons.org/licenses/by/4.0/>).

1. Introduction

Luminescent micro- or nanoparticles of wide band gap semiconductors are interesting building blocks for innovative functional materials with macroscopic dimensions, for example for optical ceramics [1–4]. This strategy may represent a valuable and cost-effective alternative to the growth of single crystals of the same material, especially when the growth of single crystals is limited with respect to accessible geometries, doping homogeneity or high temperatures [5,6]. Moreover, the intentional assembly of micro- or nanoparticles holds promises for generating particle-based macroscopic ceramics and composites, in which the particle structure and morphology can impart functionality to the assembly [7–10]. Indeed, polymer composites containing aligned alumina platelets, where the microstructure of the composite led to improved mechanical properties of the macroscopic sample were recently reported [7]. Moreover, by matching the refractive index of glass microplatelets and polymethyl methacrylate host, structurally similar materials proved to additionally gain optical transparency in the obtained composites [8,9]. A similar bottom-up approach can also be applied to other particle geometries. For example, aligned metal nanowires in a polymer matrix could be used to modify the optical properties of the composite, generating a dichroic material [10]. When functional micro- or nanomaterials are assembled without dispersing hosts, optical grade polycrystalline ceramics and composites for scintillation detection may be obtained, e.g., by using radioluminescent microparticles as building blocks [2,3,11,12]. In this scenario, doped rare earth sesquioxides (RE₂O₃) are appealing materials for phosphor or scintillation applications where light transmission is required, due to their wide band gap. Lutetia (Lu₂O₃) in particular is an interesting

candidate for ionising radiation detection, lutetium being the heaviest rare earth, ensuring high stopping power against X-rays and gamma rays. Lu_2O_3 has a band gap of around 5.8 eV, well above the visible range, and it is an ideal host for optically active rare earth dopants as it allows for substitutional doping which leads to bright radioluminescence [1,6,13–15]. Indeed, the quantum efficiency of $\text{Eu}:\text{Lu}_2\text{O}_3$ can reach up to 90% as reported for materials synthesised by combustion reactions [14]. However, the synthesis of rare earth sesquioxide particles thorough low temperature methods like solvo- or hydrothermal syntheses cannot be easily achieved. While solvothermal conditions may lead to square rare earth oxide (e.g., Gd_2O_3) nanoplatelets of around 10 nm by using acetate precursors, hydrothermal syntheses typically yield, depending on the conditions chosen, hydroxyl chloride-, hydroxide-, and oxocarbonate-microparticles, like already observed in the case of Tb, Y, and La based materials [16–19]. Synthesising such particles, an additional thermal conversion step is needed in order to form the corresponding rare earth oxides, which may impact further processing of materials based on such particles. As a consequence, these materials may represent a valuable alternative to single crystals when used as intermediate building blocks toward rare earth oxide particle-based macroscopic composites and bulk materials, provided that profitable procedures of assembly, forming, processing, and conversion into rare earth oxides can be established in order to exploit the relatively easy and cost-effective synthesis of these intermediate materials.

Considering all the above it seems clear that the control and precise understanding of the reactivity and thermal transformation of rare earth-based particles is essential to determine their suitability as constituting elements of more complex multiparticle functional materials. In this work we describe the synthesis of size-tuneable, anisotropic $\text{Eu}:\text{Lu}(\text{OH})_2\text{Cl}$ microplatelets, with special emphasis on the characterisation of their thermal evolution into highly luminescent $\text{Eu}:\text{Lu}_2\text{O}_3$, which could be an extremely versatile platform for multiparticle composites or ceramics for several optical, photonics, or scintillation applications [20,21].

2. Materials and Methods

Lutetium chloride (anhydrous, 99.99%, Sigma Aldrich, Buchs, Switzerland), benzyl alcohol (99.8%, Sigma Aldrich, Buchs, Switzerland) and Europium acetate (ABCR, Karlsruhe, Germany) were used as received without further purification.

2.1. Synthesis of $\text{Lu}(\text{OH})_2\text{Cl}$ Microcrystals

Reactions were carried out in a microwave oven (CEM, Kamp-Lintfort, Germany) using 10 mL reaction tubes. In a typical synthesis, LuCl_3 (168.8 mg, 0.6 mmol) and $\text{Eu}(\text{Ac})_3$ (6.6 mg, 0.02 mmol) were mixed with benzyl alcohol (5 mL) and sealed in an argon filled glovebox. The reaction mixtures were consequently heated in a microwave oven to either 200 °C for 1 min (sample A) or 150 °C for 5 min and 60 min (samples B and C, respectively). The resulting white precipitates were washed twice by dispersion in ethanol (2×6 mL) and diethyl ether (2×6 mL). Materials were calcined at either 500 or 1000 °C in air using a Carbolite furnace equipped with a quartz tubular chamber with a ramp rate of 10 °C/min.

2.2. Characterisation

Powder X-ray diffraction (XRD) was performed using a PANalytical Xpert Pro or Empyrean diffractometer using copper k radiation and an HTK 1200 high temperature chamber. Elemental analysis was carried out by the Laboratory of Organic Chemistry at ETH (Vladimir-Prelog-Weg 3, 8093 Zürich, Switzerland). For C, H, and N analysis a LECO TruSpec Micro (USA) system was used, while ion chromatography was employed to determine Cl. Scanning electron microscopy (SEM) was carried out using a Zeiss Leo Gemini 1530 microscope using a 3 keV electron beam. Thermogravimetric analysis (TGA) was performed using a Netzsch STA 449C instrument in the range from 25 to 1000 °C using a ramp of 10 °C min^{-1} . Transmission electron microscopy and electron diffraction was performed on a JEOL 2200fs, operating at 200 kV, and equipped with a Gatan heating holder

for in situ high temperature analysis. Photoluminescence spectroscopy was measured on a Jasco FP-8500 fluorometer equipped with a solid sample holder using emission and excitation bandwidths of 2.5 nm. Attenuated Total Reflection Infrared (ATR-IR) spectra were recorded on a Bruker Alpha-P spectrometer on solid powder samples. Optical micrographs were collected after dispersing the particles in various solvents (water, ethanol, diethyl ether) in a petri-dish through a Leica DMIL LED inverted microscope. Images of fluorescing particles were captured through a Leica DM6000B microscope equipped with a colour camera and using a 254 nm Wood-lamp as light source. Particle sizes were obtained by measuring at least 50 particles as they appeared in SEM images.

3. Results and Discussion

3.1. Synthesis of Size-Tuneable $\text{Eu:Lu(OH)}_2\text{Cl}$ Microparticles

Monoclinic lutetium dihydroxychloride ($\text{Lu(OH)}_2\text{Cl}$) anisotropic micro- and nanoparticles doped with 3 mol % were synthesised by microwave assisted non-aqueous solvothermal reactions using lutetium chloride as precursor in benzyl alcohol as a solvent. XRD analysis revealed the monoclinic crystal structure of the products, irrespective of the synthetic conditions chosen (Figure 1d) [17,22]. The product stoichiometry was further confirmed by microelemental analysis on the obtained powders, which showed a ratio of carbon (0.09), chlorine (1.0) and hydrogen (2.4) with respect to Lutetium (1.0). This result was consistent with the formation of the hydroxyl chloride, with the carbon and part of the hydrogen possibly related to traces of organic residuals at the particle surface, which often occur in solvothermal methods carried in organic media. The size of the particles could be easily controlled by tuning the synthetic parameters, namely temperature and reaction time. Mixtures heated to 200 °C for 1 min (sample A) yielded particles with average length of $8.4 \pm 3.5 \mu\text{m}$, width of $4.2 \pm 1.3 \mu\text{m}$, and a thickness of around 300 nm. At lower temperature (150 °C) 5 min of reaction were sufficient to observe the formation of smaller particles with an average length of $1.6 \pm 0.5 \mu\text{m}$, width of $0.5 \pm 0.2 \mu\text{m}$, and a thickness of around 150 nm (sample B). Longer reaction times (sample C) at lower temperature (150 °C, 60 min) further reduced the particle size to $260 \pm 10 \text{ nm}$ in length, $120 \pm 5 \text{ nm}$ in width, and thicknesses in the range 10–40 nm (Figure 1a–c). These findings revealed that higher reaction temperatures and shorter reaction times led to larger particles. Despite the growth mechanism not being fully understood, these results might indicate the initial formation of larger particles, followed by their fragmentation to form smaller particles with similar shape factors. A similar disassembly of larger particles into smaller constituent particles with identical composition has been reported elsewhere, e.g., for tungstite particles [23]. However, the exact mechanism of this non-classical crystal growth still has to be fully clarified and investigated in more depth.

All the $\text{Lu(OH)}_2\text{Cl}$ particles in this work exhibited an anisotropic, hexagonal-shaped elongated platelet morphology which was retained in both polar and unpolar solvents (Figure 1, Figures S1 and S2). This is likely due to the anisotropic unit cell of monoclinic $\text{Lu(OH)}_2\text{Cl}$, which possesses three distinct crystallographic axes *a*, *b* and *c* along which different crystal growth rates may be expected, possibly resulting in the observed morphologies [22].

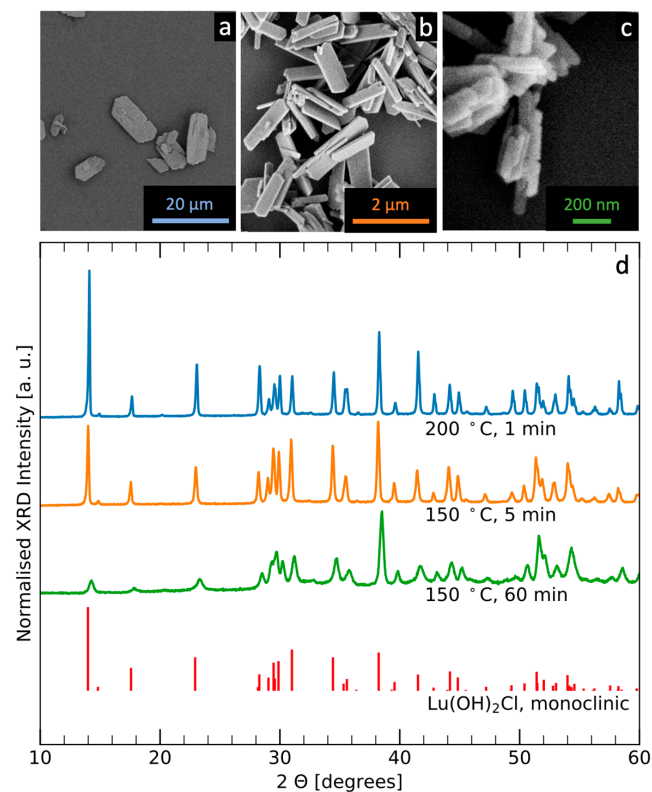
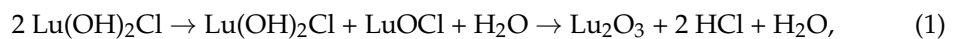


Figure 1. Role of the synthetic parameters in determining the particle morphology. (a–c) SEM micrographs of samples A, B, C respectively. (d) XRD of the samples displayed in the pictures. The diffractograms were normalised with respect to the peak at 37.9 2θ for clarity. The diffraction pattern for monoclinic $\text{Lu}(\text{OH})_2\text{Cl}$ (ICSD collection code 260838) is shown for reference.

3.2. Thermal Evolution and Formation of $\text{Eu}:\text{Lu}_2\text{O}_3$ Platelets

$\text{Eu}:\text{Lu}(\text{OH})_2\text{Cl}$ particles could be converted to $\text{Eu}:\text{Lu}_2\text{O}_3$ by calcination at 1000 °C [1,24]. The transformation of the particles' crystal structures upon exposure to heat was studied. TGA revealed three regions of weight loss upon heating up to 1000 °C, the different stages of the heat induced transformation were labelled with different colours, orange (<400 °C), green (400–650 °C) and red (>650 °C) (Figure 2a). XRD heated in situ (Figure 2b) showed that the initial monoclinic $\text{Lu}(\text{OH})_2\text{Cl}$ degraded to an intermediate product which can be at least partially associated with LuOCl before it fully turned into cubic Lu_2O_3 [22,25]. The last stage above 650 °C corresponded to the coalescence of the Lu_2O_3 crystallites. Based on the thermogravimetric analysis and the diffraction data, the stoichiometric transformations in the material upon annealing were tentatively proposed as follows:



It should be noted that the intermediate stage consisted of a mixture of species which is the reason why the diffractogram could not be fully assigned to a single specific crystal structure by XRD and ATR-IR (Figure 2b, Figure S3, Table S1). The effect of the annealing on the morphology of the particles could be further monitored during TEM experiments, where the samples were annealed in situ (Figure 2c–e). The evolution of the crystal structure of single microplatelets could be observed. Initially, the platelets exhibited lamellar structures along the edge, which disappeared when the $\text{Lu}(\text{OH})_2\text{Cl}$ was transformed to polycrystalline Lu_2O_3 , above 800 °C (Figure S4). The lamellar periodicity in as synthesised microparticles was measured to be around 1 nm (Figure S5). This distance could not be correlated to any of the lattice parameters of $\text{Lu}(\text{OH})_2\text{Cl}$. Therefore, its origin might be due to layers rich in oxygen, hydrogen and chlorine intercalated with layers rich in lutetium as it was observed in mixed crystal lamellar structures [26]. The overall morphology of the

microplatelet was not affected by the heat treatment (Figure 2e). This is also shown by SEM micrographs of platelets after ex situ annealing at 1000 °C (Figure 2f, Figure S4). While the surface roughness of the platelets was enhanced due to the polycrystalline nature of the newly formed Lu_2O_3 and due to the change of density of the initial and final crystal structure, the overall initial platelet morphology was retained in all directions. Therefore, the transformation of $\text{Eu}:\text{Lu}(\text{OH})_2\text{Cl}$ platelets into $\text{Eu}:\text{Lu}_2\text{O}_3$ platelets represents a useful type of morphological control for cubic Lu_2O_3 , appearing as a promising tool to design multiparticle assemblies which can be treated at high temperature without catastrophic shrinkage or structural rearrangement, which typically are the main source of difficulties in ceramic powder processing.

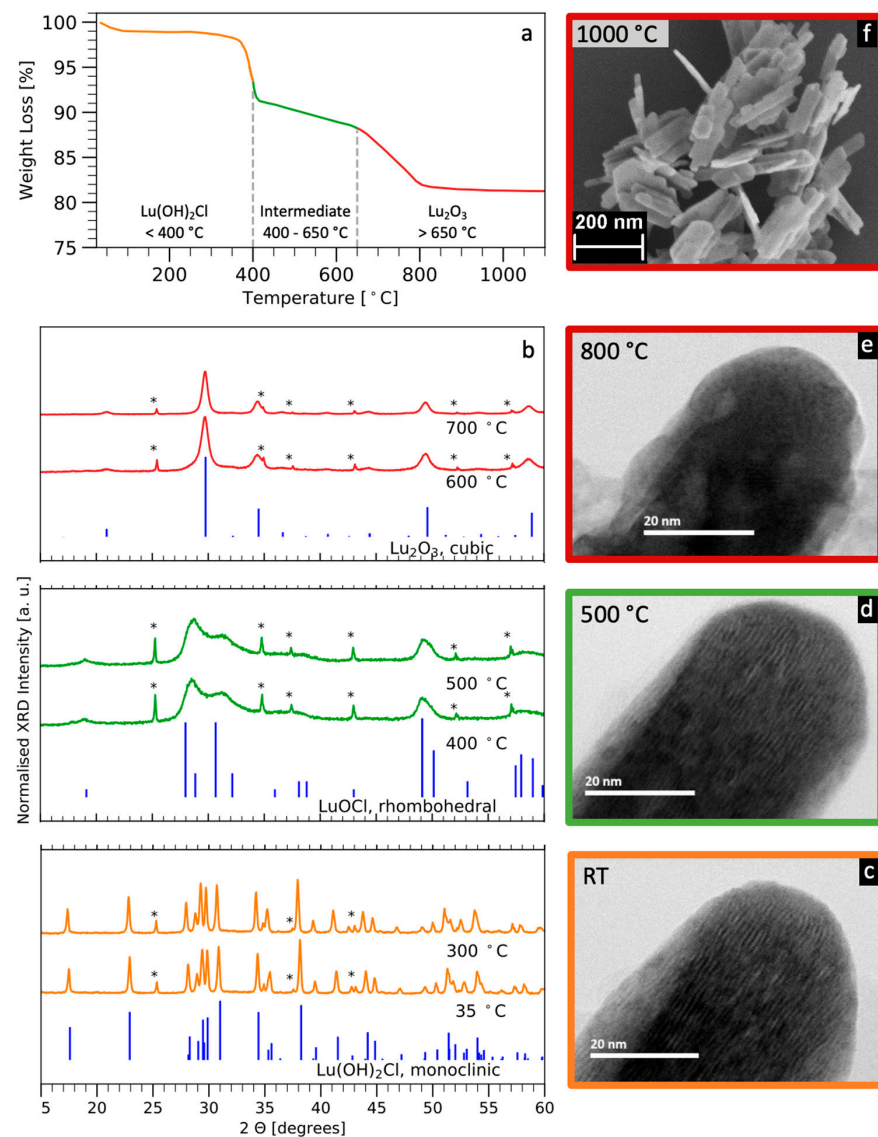


Figure 2. Thermal evolution of $\text{Eu}:\text{Lu}(\text{OH})_2\text{Cl}$ platelets (sample C). (a) TGA. (b) In situ high temperature XRD (peaks corresponding to the corundum substrate are marked with asterisks *). The colours orange, green and red label different temperature stages: <400, 400–650, >650 °C, respectively. $\text{Lu}(\text{OH})_2\text{Cl}$ ICSD collection code 260838, LuOCl PDF code 00-035-1344, Lu_2O_3 ICSD collection code 40471 are displayed for reference. (c–e) In situ heating TEM micrographs of the same platelet seen through its edge, recorded at room temperature, at 500 and at 800 °C, respectively. (f) SEM of powder calcined at 1000 °C.

3.3. Luminescence

Due to its full 4f-shell, Lu^{3+} is an optically inactive rare earth ion. Consequently, Lu_2O_3 is a PL-silent material which can be activated by doping with optically active rare earth elements [27,28]. The PL spectra of untreated, semi-calcined, and calcined powders showed clear differences in terms of transitions ratios and intensities, as expected by considering the strict dependence on the lattice site geometry typically expressed by the emission profile of europium (Figure 3) [27,29]. The emission profile of $\text{Eu:Lu(OH)}_2\text{Cl}$ particles was in good agreement with the one reported for $\text{Eu(OH)}_2\text{Cl}$ [30]. A blue luminescence associated to organic side-products resulting from the polymerisation of benzyl alcohol could be observed in $\text{Eu:Lu(OH)}_2\text{Cl}$ samples (Figure S6). Considering the lower crystal grade associated with broader XRD peaks of the intermediate compound (Figure 2b), one could expect a inhomogeneous broadening of the europium(III) emission [27]. However, this broadening is not very evident in the recorded PL spectra. The $\text{Eu:Lu}_2\text{O}_3$ particles obtained after calcination expressed bright red luminescence under UV excitation even after being redispersed in water (Figure S7).

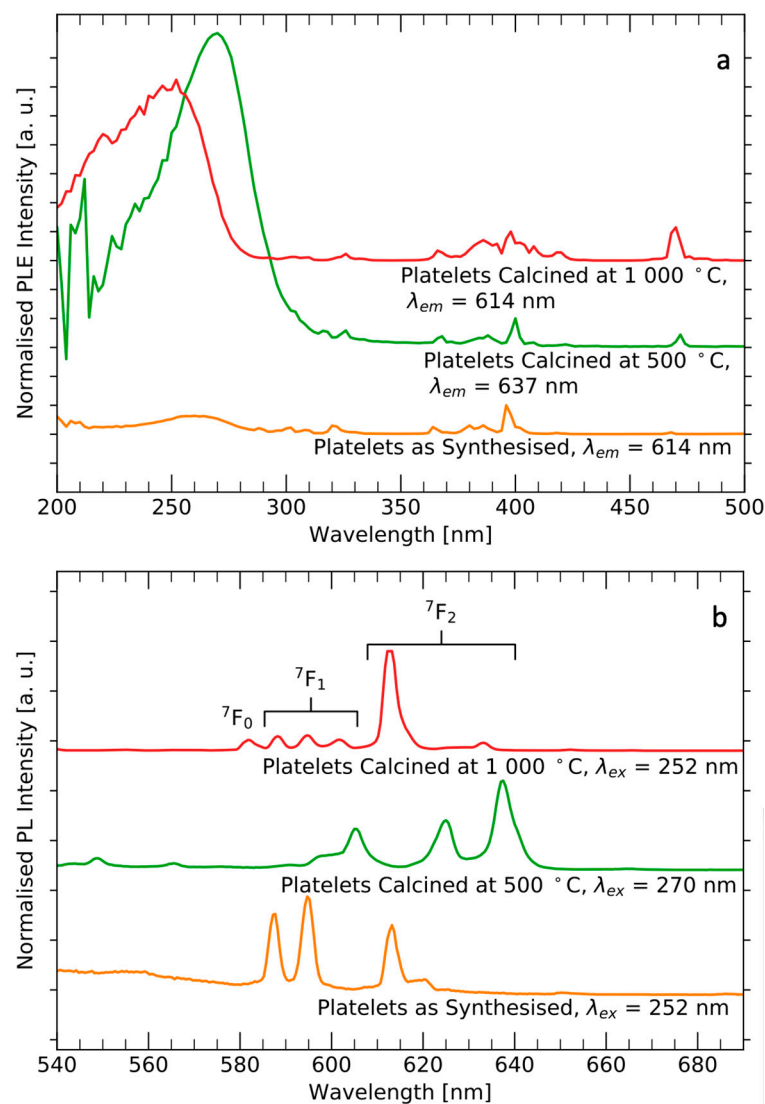


Figure 3. Effect of annealing on the Eu^{3+} related luminescence. (a) PLE spectra of $\text{Eu:Lu(OH)}_2\text{Cl}$, the intermediate and the final product $\text{Eu:Lu}_2\text{O}_3$. Emission wavelengths were 614, 637 and 614 nm, respectively. Spectra were normalised at 394 nm. (b) PL of initial product, intermediate and final product, $\lambda_{ex} = 252, 270$ and 252 nm, respectively. All spectra were normalised for the most intense peak.

4. Conclusions

We report the controlled, solvothermal synthesis of Lu(OH)₂Cl particles and the thermal evolution of the material rendering Lu₂O₃ above 800 °C. The particle size could be readily controlled by varying synthetic parameters such as temperature and time while the crystal structure remained the same. Composition and structure of the europium doped platelets however changed dramatically with annealing. The decomposition of Lu(OH)₂Cl to Lu₂O₃ was also reflected in the photoluminescence emission spectra of the initial and final microparticles. In summary, an up to now unknown level of morphology control of Eu:Lu(OH)₂Cl micromaterials which could be transformed to Eu:Lu₂O₃ was demonstrated. Since Lu₂O₃ is technologically important for applications such as X-ray and γ -ray detection, these results pave the way towards microstructurally controlled ceramic- and composite-materials [20,21].

Supplementary Materials: The following are available online at <https://www.mdpi.com/article/10.3390/cryst11080992/s1>, Supporting Information.pdf.

Author Contributions: Conceptualization, A.L.; Data curation, M.F. and A.L.; Investigation, M.F., A.S. and A.L.; Methodology, A.L.; Project administration, A.L.; Supervision, A.L.; Visualization, M.F., A.S. and A.L.; Writing—original draft, M.F.; Writing—review & editing, M.F. and A.L. All authors have read and agreed to the published version of the manuscript.

Funding: This research received no external funding.

Acknowledgments: The authors are grateful to ETH Zürich for the financial support and to Gabriele Ilari (Electron Microscopy Center, Swiss Federal Laboratories for Materials Science and Technology, Empa) for the TEM data. Furthermore, the Complex Materials group at the department of Materials at ETH Zürich is acknowledged for providing access to optical microscopes.

Conflicts of Interest: The authors declare no conflict of interest.

References

1. Seeley, Z.M.; Kuntz, J.D.; Cherepy, N.J.; Payne, S.A. Transparent Lu₂O₃:Eu ceramics by sinter and HIP optimization. *Opt. Mater.* **2011**, *33*, 1721–1726. [[CrossRef](#)]
2. Satapathy, S.; Ahlawat, A.; Paliwal, A.; Singh, R.; Singh, M.K.; Gupta, P.K. Effect of calcination temperature on nanoparticle morphology and its consequence on optical properties of Nd:Y₂O₃ transparent ceramics. *CrystEngComm.* **2014**, *16*, 2723–2731. [[CrossRef](#)]
3. Serrano, A.; Caballero-Calero, O.; García, M.Á.; Lazić, S.; Carmona, N.; Castro, G.R.; Martín-González, M.; Fernández, J.F. Cold sintering process of ZnO ceramics: Effect of the nanoparticle/microparticle ratio. *J. Eur. Ceram. Soc.* **2020**, *40*, 5535–5542. [[CrossRef](#)]
4. Massera, J.; Gaussiran, M.; Gluchowski, P.; Lastusaari, M.; Hupa, L.; Petit, L. Processing and characterization of phosphate glasses containing CaAl₂O₄:Eu²⁺,Nd³⁺ and SrAl₂O₄:Eu²⁺,Dy³⁺ microparticles. *J. Eur. Ceram. Soc.* **2015**, *35*, 3863–3871. [[CrossRef](#)]
5. Vanecek, V.; Kral, R.; Paterek, J.; Babin, V.; Jary, V.; Hybler, J.; Kodama, S.; Kurosawa, S.; Yokota, Y.; Yoshikawa, A.; et al. Modified vertical Bridgman method: Time and cost effective tool for preparation of Cs₂HfCl₆ single crystals. *J. Cryst. Growth* **2020**, *533*, 125479. [[CrossRef](#)]
6. Guzik, M.; Pejchal, J.; Yoshikawa, A.; Ito, A.; Goto, T.; Siczek, M.; Lis, T.; Boulon, G. Structural investigations of Lu₂O₃ as single crystal and polycrystalline transparent ceramic. *Cryst. Growth Des.* **2014**, *14*, 3327–3334. [[CrossRef](#)]
7. Erb, R.M.; Libanori, R.; Rothfuchs, N.; Studart, A.R. Composites Reinforced in Three Dimensions by Using Low Magnetic Fields. *Science* **2012**, *335*, 199–204. [[CrossRef](#)]
8. Magrini, T.; Bouville, F.; Lauria, A.; Le Ferrand, H.; Niebel, T.P.; Studart, A.R. Transparent and tough bulk composites inspired by nacre. *Nat. Commun.* **2019**, *10*, 2794. [[CrossRef](#)]
9. Magrini, T.; Moser, S.; Fellner, M.; Lauria, A.; Bouville, F.; Studart, A.R. Transparent Nacre-like Composites Toughened through Mineral Bridges. *Adv. Funct. Mater.* **2020**, *30*, 2002149. [[CrossRef](#)]
10. Nydegger, M.; Deshmukh, R.; Tervoort, E.; Niederberger, M.; Caseri, W. Composites of Copper Nanowires in Polyethylene: Preparation and Processing to Materials with NIR Dichroism. *ACS Omega* **2019**, *4*, 11223–11228. [[CrossRef](#)] [[PubMed](#)]
11. Chernenko, K.A.; Gorokhova, E.I.; Eronko, S.B.; Sandulenko, A.V.; Venetsev, I.D.; Wiczorek, H.; Rodnyi, P.A. Structural, Optical, and Luminescent Properties of ZnO:Ga and ZnO:In Ceramics. *IEEE Trans. Nucl. Sci.* **2018**, *65*, 2196–2202. [[CrossRef](#)]
12. Shmurak, S.Z.; Kedrov, V.V.; Klassen, N.V.; Shakhrai, O.A. Spectroscopy of composite scintillators. *Phys. Solid State* **2012**, *54*, 2266–2276. [[CrossRef](#)]

13. Kalyvas, N.; Liaparinos, P.; Michail, C.; David, S.; Fountos, G.; Wójtowicz, M.; Zych, E.; Kandarakis, I. Studying the luminescence efficiency of $\text{Lu}_2\text{O}_3:\text{Eu}$ nanophosphor material for digital X-ray imaging applications. *Appl. Phys. A* **2012**, *106*, 131–136. [[CrossRef](#)]
14. Zych, E.; Meijerink, A.; De, C.; Donegá, M. Quantum efficiency of europium emission from nanocrystalline powders of $\text{Lu}_2\text{O}_3:\text{Eu}$. *J. Phys. Condens. Matter* **2003**, *15*, 5145–5155. [[CrossRef](#)]
15. Zych, E.; Trojan-Piegza, J. Low-Temperature Luminescence of $\text{Lu}_2\text{O}_3:\text{Eu}$ Ceramics upon Excitation with Synchrotron Radiation in the Vicinity of Band Gap Energy. *Chem. Mater.* **2006**, *18*, 2194–2199. [[CrossRef](#)]
16. Cao, Y.C. Synthesis of Square Gadolinium-Oxide Nanoplates. *J. Am. Chem. Soc.* **2004**, *126*, 7456–7457. [[CrossRef](#)]
17. Mahajan, S.V.; Hart, J.; Hood, J.; Everheart, A.; Redigolo, M.L.; Koktysh, D.S.; Payzant, E.A.; Dickerson, J.H. Synthesis of $\text{RE}(\text{OH})_2\text{Cl}$ and REOCl ($\text{RE}=\text{Eu}, \text{Tb}$) nanostructures. *J. Rare Earths* **2008**, *26*, 131–135. [[CrossRef](#)]
18. Fang, Y.-P.; Xu, A.-W.; You, L.-P.; Song, R.-Q.; Yu, J.C.; Zhang, H.-X.; Li, Q.; Liu, H.-Q. Hydrothermal Synthesis of Rare Earth (Tb, Y) Hydroxide and Oxide Nanotubes. *Adv. Funct. Mater.* **2003**, *13*, 955–960. [[CrossRef](#)]
19. Li, G.; Peng, C.; Zhang, C.; Xu, Z.; Shang, M.; Yang, D.; Kang, X.; Wang, W.; Li, C.; Cheng, Z.; et al. $\text{Eu}^{3+}/\text{Tb}^{3+}$ -Doped $\text{La}_2\text{O}_2\text{CO}_3/\text{La}_2\text{O}_3$ Nano/Microcrystals with Multiform Morphologies: Facile Synthesis, Growth Mechanism, and Luminescence Properties. *Inorg. Chem.* **2010**, *49*, 10522–10535. [[CrossRef](#)]
20. Liu, J.; Liu, B.; Zhu, Z.; Chen, L.; Hu, J.; Xu, M.; Cheng, C.; Ouyang, X.; Zhang, Z.; Ruan, J.; et al. Modified timing characteristic of a scintillation detection system with photonic crystal structures. *Opt. Lett.* **2017**, *42*, 987–990. [[CrossRef](#)]
21. Knapitsch, A.; Auffray, E.; Fabjan, C.W.; Leclercq, J.L.; Lecoq, P.; Letartre, X.; Seassal, C. Photonic crystals: A novel approach to enhance the light output of scintillation based detectors. *Nucl. Instrum. Methods Phys. Res.* **2011**, *628*, 385–388. [[CrossRef](#)]
22. Zehnder, R.A.; Clark, D.L.; Scott, B.L.; Donohoe, R.J.; Palmer, P.D.; Runde, W.H.; Hobart, D.E. Investigation of the Structural Properties of an Extended Series of Lanthanide Bis-hydroxychlorides $\text{Ln}(\text{OH})_2\text{Cl}$ ($\text{Ln} = \text{Nd} - \text{Lu}$, except Pm and Sm). *Inorg. Chem.* **2010**, *49*, 4781–4790. [[CrossRef](#)]
23. Olliges-Stadler, I.; Rossell, M.D.; Süess, M.J.; Ludi, B.; Bunk, O.; Pedersen, J.S.; Birkedal, H.; Niederberger, M. A comprehensive study of the crystallization mechanism involved in the nonaqueous formation of tungstite. *Nanoscale* **2013**, *5*, 8517. [[CrossRef](#)]
24. Thoř, T.; Rubeřová, K.; Jakeř, V.; Cajzl, J.; Nádherný, L.; Mikolášová, D.; Kučerková, R.; Nikl, M. Lanthanide-doped Lu_2O_3 phosphors and scintillators with green-to-red emission. *J. Lumin.* **2019**, *215*, 116647. [[CrossRef](#)]
25. Brandt, G.; Diehl, R. Preparation, powder data and crystal structure of YbOCl . *Mater. Res. Bull.* **1974**, *9*, 411–419. [[CrossRef](#)]
26. Pinna, N.; Garnweitner, G.; Beato, P.; Niederberger, M.; Antonietti, M. Synthesis of Yttria-Based Crystalline and Lamellar Nanostructures and their Formation Mechanism. *Small* **2004**, *1*, 112–121. [[CrossRef](#)]
27. Binnemans, K. Interpretation of europium(III) spectra. *Coord. Chem. Rev.* **2015**, *295*, 1–45. [[CrossRef](#)]
28. Lauria, A.; Chiodini, N.; Fasoli, M.; Mihóková, E.; Moretti, F.; Nale, A.; Nikl, M.; Vedda, A. Acetate–citrate gel combustion: A strategy for the synthesis of nanosized lutetium hafnate phosphor powders. *J. Mater. Chem.* **2011**, *21*, 8975. [[CrossRef](#)]
29. Boyer, J.C.; Vetrone, F.; Capobianco, J.A.; Speghini, A.; Bettinelli, M. Variation of Fluorescence Lifetimes and Judd-Ofelt Parameters between Eu^{3+} Doped Bulk and Nanocrystalline Cubic Lu_2O_3 . *J. Phys. Chem. B* **2004**, *108*, 20137–20143. [[CrossRef](#)]
30. Mahajan, S.V.; Redigolo, M.L.; Koktysh, D.S.; Dickerson, J.H. Stepwise assembly of europium sesquioxide nanocrystals and nanoneedles. In Proceedings of the Nanophotonic Materials III, San Diego, CA, USA, 13–17 August 2006; Gaburro, Z., Cabrini, S., Eds.; Volume 6321, p. 632102.